GEOPHYSICS, VOL. 71, NO. 3 (MAY-JUNE 2006); P. D93–D105, 15 FIGS., 2 TABLES.
10.1190/1.2196872

Seismic characterization of multiple fracture sets: Does orthotropy suffice?

Vladimir Grechka[1] and Mark Kachanov[2]

ABSTRACT

As geophysicists rely increasingly on effective media theories to characterize naturally fractured reservoirs, they become more and more interested in evaluating the accuracy of different theories, estimating their limits of applicability, and assessing their usefulness for practice. With this in mind, we compare two popular seismological theories of Hudson and Schoenberg with the theory of Kachanov developed in the context of mechanics of materials. By performing finite-element simulations of effective media for models that contain several sets of nonintersecting, circular, vertical fractures embedded in otherwise isotropic host rock, we examine the accuracy of these theories. Our numeric study reveals that predictions of both the first- and second-order Hudson's theories are typically inferior to those of others, especially when the fractures are dry. While, on average, the theories of Schoenberg and Kachanov fit finite-element computations with comparable accuracy, the latter appears to be more useful for fracture characterization. The reason is that it correctly predicts the proximity of crack-induced anisotropy to orthotropy, whereas the other theories do not. Kachanov's results not only yield approximate effective orthotropy regardless of the number of fracture sets, their crack densities, and orientations, but they also lead to a substantially reduced number of independent parameters that govern the effective stiffnesses. This number is only four for dry cracks, compared to nine required for general orthorhombic media. These four quantities can be chosen as two Lamé constants of the isotropic background and two principal crack densities. If fractures are filled with a compressible fluid, the number of independent parameters increases. After numeric verification of the accuracy of crack-induced orthotropy, we invert the NMO ellipses and zero-offset traveltimes of P-waves and two split shear waves for the parameters characterizing multiple fracture sets. Our inversion reveals the fracture parameters that can be unambiguously estimated from multiazimuth, multicomponent surface reflection data.

INTRODUCTION

The almost ubiquitous presence of fractures in the subsurface and their tendency to provide natural pathways for hydrocarbon flow makes them an important target in the exploration and exploitation of oil and gas reservoirs. Seismic data typically can image only relatively large faults whose size is greater than or comparable with the seismic wavelengths. Many smaller fractures of exploration interest that have subseismic lengths cannot be imaged directly, and nearly all information about them is inferred from seismic data by applying some effective media theories. Thus, developing sufficiently accurate effective media theories becomes a critically important task when characterizing fractures.

The problem of finding the effective elastic properties of cracked materials was first addressed, in the general context of solid mechanics, by Bristow (1960) and, in the context of rock mechanics, by Walsh (1965a, b). Both developments rested on two assumptions: (1) the elastic interactions between cracks were neglected (the so-called noninteraction approximation) and (2) the crack orientations were assumed to be random, resulting in the overall isotropy. Importantly, both Bristow (1960) and Walsh (1965a, b) identified scalar crack density as the parameter governing the effective elastic constants.

Kachanov (1980) extends the noninteraction approximation to general effective anisotropy, attributable to arbitrarily oriented circular dry cracks embedded in an otherwise isotropic background. He draws a somewhat counterintuitive conclusion: The effective elasticity is approximately orthorhombic (orthotropic) for any orientational distribution of the fractures. Moreover, the orthotropy turns out to be of a simplified type, with the number of independent

Manuscript received by the Editor April 18, 2005; revised manuscript received October 17, 2005; published online May 26, 2006.
[1]Shell International Exploration and Production, Inc., 3737 Bellaire Blvd., P. O. Box 481, Houston, Texas, 77001-0481. E-mail: vladimir.grechka@shell.com.
[2]Tufts University, Department of Mechanical Engineering, Medford, Massachusetts 02155. E-mail: mark.kachanov@tufts.edu.

constants reduced from nine to only four. These results point to the proper crack-density parameters — a second-rank crack density tensor that generalizes the scalar crack density and a fourth-rank tensor.

The discussed noninteraction approximation is rigorously correct at small crack densities when fracture interactions in the stress and strain fields can be ignored. At higher crack densities, the local interactions become strong and might contribute to the effective elasticity (Grechka, 2005). The overall influence of interactions, however, seems to be less pronounced when multiple, differently oriented fracture sets are present because the shielding interactions, which dominate for stacked arrangements, and the amplifying interactions, which tend to take over for coplanar cracks, produce opposite effects that nearly cancel each other (Kachanov, 1992, 1993). The noninteraction approximation also deserves discussion for another reason: Many effective media schemes (self-consistent, differential, etc.) utilize it as a basic building block (Mori and Tanaka, 1973; O'Connell and Budiansky, 1974; Benveniste, 1986).

In seismic exploration where a parallel work took place, two popular effective media theories have been proposed by Hudson (1980) and Schoenberg (1980). These theories originally were developed for a single set of rotationally invariant cracks embedded in isotropic host rock and later were extended to several fracture sets (e.g., Hudson 1981; Nichols et al., 1989; Schoenberg and Muir, 1989; Jakobsen et al., 2003) and to anisotropic backgrounds (e.g., Schoenberg and Helbig, 1997; Bakulin et al., 2000; Grechka and Tsvankin, 2003). Both the developments of Hudson (1980) and Schoenberg (1980) and their multiple extensions are not exact for a finite crack density; they are approximations based on certain additional assumptions. An approximate nature of the effective media theories leads to the first goal of our paper: numerical verification of their accuracy. Once accuracy is established and the best theories are selected, our second, more practical goal emerges: We invert seismic signatures for proper combinations of the microstructural parameters that control the effective stiffnesses. This inversion process is known as fracture characterization.

The predictions of effective-media theories can be verified by direct computations of effective elasticity done on sufficient numbers of crack arrays. Such studies have been published for randomly oriented cracks (Kachanov, 1992; Saenger et al., 2004) and for a single fracture set (Grechka, 2005). Here we continue this general line of work. Since direct measurements of fracture distributions (for instance, core analysis, outcrop studies, and borehole televiewer data) typically indicate the presence of multiple fracture sets, we build numeric models that contain several sets of vertical, nonintersecting, and noninterconnected fractures. To test the effective-media theories and eliminate the complicating issues of various crack shapes, we choose fractures that are thin, circular ellipsoids. With these simplified models of cracks, we analyze the accuracy of the first- and second-order theories of Hudson (1980, 1994), the linear slip theory of Schoenberg (1980), and the theory of Kachanov (1980). The latter predicts that the symmetry of effective anisotropy induced by dry cracks is close to orthorhombic regardless of the number of fracture sets, their crack densities, and their orientations, whereas the other theories do not identify this symmetry.

Being numerically verified, effective orthotropy becomes an extremely useful property for fracture characterization because it significantly reduces the number of quantities that control the seismic signatures. We numerically confirm the theoretical conclusion of Kachanov (1993) that, for dry vertical cracks, the effective stiffnesses are governed by only four, rather than nine independent parameters. We choose these parameters to be two Lamé constants of the isotropic background and two principal crack densities. Furthermore, we show that these parameters can be estimated uniquely from multiazimuth, multicomponent seismic reflection data.

Our paper is organized in the following way: First, we give an overview of theoretical results of Kachanov (1980, 1992, 1993), Schoenberg (1980), and Hudson (1980, 1981). Then, we compare their theoretical predictions with finite-element simulations of effective media (done with FEMLAB software; Comsol, 2006). We conclude that the orthotropic approximation of Kachanov (1980, 1992, 1993) is supported by numeric modeling and proceed with estimating parameters governing the crack-induced orthotropy from the P- and split shear-wave NMO ellipses.

NONINTERACTION APPROXIMATION FOR FRACTURED MEDIA

Circular dry fractures

The quantities governing the influence of cracks on effective elasticity are most easily identified from the elastic potential f, whose derivative with respect to the stress is the strain. If a solid contains many circular fractures of diverse orientation and size, and interactions in the stress fields of the adjacent cracks are ignored, the fracture contribution Δf to the elastic potential has the form (Kachanov, 1980, 1992)

$$\Delta f = \frac{16(1-\nu^2)}{3E(2-\nu)}[(\boldsymbol{\tau}\cdot\boldsymbol{\tau}):\boldsymbol{\alpha} + \boldsymbol{\tau}:\boldsymbol{\beta}:\boldsymbol{\tau}]. \qquad (1)$$

Here, ν is the background Poisson's ratio, E is the Young's modulus, $\boldsymbol{\tau}$ is the remotely applied stress, the colon denotes a double dot product (a contraction over two indices),

$$\boldsymbol{\alpha} = \frac{1}{V}\sum_k (a^3\mathbf{nn})^{(k)} \qquad (2)$$

is the symmetric second-rank crack-density tensor, and

$$\boldsymbol{\beta} = -\frac{\nu}{2}\frac{1}{V}\sum_k (a^3\mathbf{nnnn})^{(k)} \qquad (3)$$

is the fourth-rank tensor that emerges as another crack-density parameter. The sums in equations 2 and 3 are taken with respect to all fractures k in the representative rock volume V, $a^{(k)}$ are the crack radii, and $\mathbf{n}^{(k)}$ are the unit normals to the crack faces.

Tensors $\boldsymbol{\alpha}$ and $\boldsymbol{\beta}$ contain all of the information about the crack statistics — the distribution over orientations and size — relevant for the effective properties in the noninteraction approximation. The crack openings, or the aspect ratios do not enter equations 1–3. Thus, the effective properties of solids with dry cracks are almost independent of the aspect ratios, provided that the latter are small.

The influence of $\boldsymbol{\beta}$ in equation 1 is relatively minor because of the multiplier $\nu/2 < 1/4$ (equation 3). Hence, neglecting this term and retaining $\boldsymbol{\alpha}$ as the sole crack-density parameter is a satisfactory approximation. Since $\boldsymbol{\alpha}$ is the symmetric second-rank tensor, a solid with arbitrarily oriented circular cracks is approximately orthor-

hombic, and the axes of crack-induced orthotropy approximately coincide with the principal directions of $\boldsymbol{\alpha}$. Moreover, this orthotropy is close to elliptical and is characterized by the background parameters E and ν (or, equivalently, Lamé constants λ_b and μ_b) and three eigenvalues of tensor $\boldsymbol{\alpha}$. Schoenberg and Sayers (1995) call such fractures scalar. For vertical fractures examined later, one of those eigenvalues is zero and the effective orthotropy is governed by only four rather than nine independent parameters.

Equation 1 can be rewritten for the extra compliance because of cracks (Kachanov, 1980; Sayers and Kachanov, 1995; Schoenberg and Sayers, 1995)

$$\Delta s_{ijlm} = \frac{8(1-\nu^2)}{3E(2-\nu)}(\alpha_{il}\delta_{jm} + \alpha_{im}\delta_{jl} + \alpha_{jl}\delta_{im} + \alpha_{jm}\delta_{il} + 4\beta_{ijlm}), \quad (i,j,l,m = 1,2,3), \tag{4}$$

where δ_{jm} is the Kronecker delta. Approximating the components β_{ijlm} in equation 4 with $-\nu(\alpha_{il}\delta_{jm} + \alpha_{im}\delta_{jl} + \alpha_{jl}\delta_{im} + \alpha_{jm}\delta_{il})/8$, we obtain the effective elliptical orthotropy,

$$\Delta \boldsymbol{s}^{\text{ell}} = \frac{16}{3E}(1-\nu^2)\boldsymbol{\alpha}. \tag{5}$$

Liquid-filled fractures

The influence of liquid infill on the overall compliance is described by Kachanov (1992, 1993) and Shafiro and Kachanov (1997). They generalize equation 4 to

$$\Delta s_{ijlm} = \frac{8(1-\nu^2)}{3E(2-\nu)}(\alpha_{il}\delta_{jm} + \alpha_{im}\delta_{jl} + \alpha_{jl}\delta_{im} + \alpha_{jm}\delta_{il} + 4\beta'_{ijlm}), \quad (i,\, j,\, l,\, m = 1,2,3), \tag{6}$$

where

$$\boldsymbol{\beta}' = \boldsymbol{\beta} - \frac{1}{V}\left(1 - \frac{\nu}{2}\right)\sum_k (\varsigma a^3 \boldsymbol{nnnn})^{(k)}. \tag{7}$$

The dimensionless parameters $\varsigma^{(k)}$, called the fluid factors, account for the infill of the kth crack. They are given by

$$\varsigma^{(k)} = \frac{1}{1 + \theta^{(k)}[E/K - 3(1-2\nu)}, \tag{8}$$

where K is the bulk modulus of the fluid and $\theta^{(k)}$ are the crack aspect ratios.

Equations 6–8 allow us to identify two important complications introduced by the presence of fluids in cracks. First, the fluid factors $\varsigma^{(k)}$ are not small compared to unity; consequently, $\boldsymbol{\alpha}$ and $\boldsymbol{\beta}'$ (equations 2 and 7) have comparable magnitudes. Therefore, $\boldsymbol{\beta}'$ cannot be ignored and the effective orthotropy may be lost, making the overall symmetry lower than orthorhombic. Second, individual contributions of liquid-filled cracks to the effective compliance strongly depend on their aspect ratios $\theta^{(k)}$, which may be as diverse as the crack radii $a^{(k)}$. These additional microstructural parameters are captured by the fourth-rank tensor $\boldsymbol{\beta}'$; however, their estimation from the effective properties is obviously ambiguous.

EFFECTIVE-MEDIA THEORIES

Next, we discuss the effective-media theories for L sets of vertical cracks embedded in otherwise isotropic host rock. We denote the orientation of each set by vector $\boldsymbol{n}^{(\ell)}$ ($\ell = 1, \dots, L$) and the number of fractures there by L_ℓ. Then, equation 2 yields the partial crack densities

$$e_\ell = \sum_{k=1}^{L_\ell} \frac{(a^3)^{(k)}}{V} \tag{9}$$

for each fracture set.

Kachanov's theory

The effective compliance tensor of the fractured material is represented as a sum

$$\boldsymbol{s}_e^{\text{K}} = \boldsymbol{s}_b + \Delta \boldsymbol{s}. \tag{10}$$

where K stands for Kanchanov. Here, $\boldsymbol{s}_b$ is the background compliance tensor and the fourth-rank tensor $\Delta \boldsymbol{s}$ is given by equation 6 (Kachanov, 1980, 1993; Kachanov and Sevostianov, 2005). For L vertical fracture sets, tensors $\boldsymbol{\alpha}$ and $\boldsymbol{\beta}$ (equations 2 and 3), take the form

$$\boldsymbol{\alpha} = \sum_{\ell=1}^{L} e_\ell (\boldsymbol{nn})^{(\ell)}, \tag{11}$$

$$\boldsymbol{\beta} = -\frac{\nu}{2}\sum_{\ell=1}^{L} e_\ell (\boldsymbol{nnnn})^{(\ell)}, \tag{12}$$

where e_ℓ are the partial crack densities (equation 9) associated with each fracture set.

Tensor $\boldsymbol{\beta}'$ does not depend solely on e_ℓ when distributions of the crack radii $a^{(k)}$ and the fluid factors $\varsigma^{(k)}$ are correlated. Assuming that $\boldsymbol{n}^{(\ell)}$ $a^{(k)}$ and $\varsigma^{(k)}$ are uncorrelated, we rewrite equation 7 in a form similar to equation 12,

$$\boldsymbol{\beta}' = \boldsymbol{\beta} - \left(1 - \frac{\nu}{2}\right)\varsigma \sum_{\ell=1}^{L} e_\ell (\boldsymbol{nnnn})^{(\ell)}, \tag{13}$$

where $\varsigma = \text{mean}(\varsigma^{(k)})$.

Dry fractures: Approximate effective orthotropy

For dry fractures, whose infill has the zero bulk modulus K, fluid factors $\varsigma^{(k)}$ defined by equation 8 disappear and $\boldsymbol{\beta}' = \boldsymbol{\beta}$. As a result, the contribution of cracks $\Delta \boldsymbol{s}$ to the effective compliance is given by equation 4. As we have discussed, it can be approximated by the effective elliptical orthotropy (equation 5), which yields the effective compliance tensor

$$\boldsymbol{s}^{\mathrm{K,ell}} = \boldsymbol{s}_b + \Delta\boldsymbol{s}^{\mathrm{ell}}. \tag{14}$$

The effective orthorhombic anisotropy implied by equation 14 is of a special type. It can be fully characterized by only four independent quantities rather than by the nine needed for general orthotropy (Kachanov, 1992, 1993). For vertical cracks, these quantities can be chosen as the background Lamé parameters λ_b and μ_b and as two nonzero eigenvalues $\widetilde{e}_1$ and $\widetilde{e}_2$ of the crack-density tensor $\boldsymbol{\alpha}$. We call $\widetilde{e}_1$ and $\widetilde{e}_2$ the principal crack densities.

Liquid-filled fractures

The noninteraction approximation predicts two types of issues caused by the presence of compressible fluid infill in cracks. First, comparable magnitudes of tensors $\boldsymbol{\beta}'$ and $\boldsymbol{\alpha}$ imply that effective orthotropy might be violated. However, this may not be important because these tensors partially compensate each other, yielding an overall weaker anisotropy than that for dry cracks. The net result is that anisotropy of $\boldsymbol{s}_e^{\mathrm{K}}$ is close to orthotropy again, but this time, mainly because of its proximity to isotropy. We present a numeric verification of this statement later. Second, the crack aspect ratios $\theta^{(k)}$, which become important parameters in the presence of fluid (Shafiro and Kachanov, 1997), cannot be estimated uniquely from the effective elastic constants if these aspect ratios are diverse. Still, extracting some average fluid factor ς would be useful for fracture characterization. We introduce it with equation 13. The estimated value of ς is expected to be close to zero if cracks are dry or have sufficiently large $\theta^{(k)}$ (so that the influence of fluid is weak) and close to unity if the liquid-filled fractures are narrow.

The fact of approximate effective orthotropy can be exploited further by replacing multiple vertical fracture sets with two orthogonal ones that have some effective crack densities $\widetilde{e}_1$ and $\widetilde{e}_2$. In the rotated coordinate frame whose axes coincide with the normals to these two fracture sets, equation 10 takes the form

$$\boldsymbol{s}_e^{\mathrm{K,orth}} = \boldsymbol{s}_b + \Delta\boldsymbol{s}^{\mathrm{orth}}. \tag{15}$$

The nonzero elements of tensor $\Delta\boldsymbol{s}^{\mathrm{orth}}$ are

$$\Delta s_{11}^{\mathrm{orth}} = \frac{16\widetilde{e}_1(1-\nu^2)}{3E}(1-\varsigma),\quad \Delta s_{55}^{\mathrm{orth}} = \frac{32\widetilde{e}_1(1-\nu^2)}{3E(2-\nu)},$$

$$\Delta s_{22}^{\mathrm{orth}} = \frac{16\widetilde{e}_2(1-\nu^2)}{3E}(1-\varsigma),\quad \Delta s_{44}^{\mathrm{orth}} = \frac{32\widetilde{e}_2(1-\nu^2)}{3E(2-\nu)},$$

$$\Delta s_{66}^{\mathrm{orth}} = \Delta s_{44}^{\mathrm{orth}} + \Delta s_{55}^{\mathrm{orth}}. \tag{16}$$

Schoenberg's theory

The linear slip theory of Schoenberg (1980) has many similarities with Kachanov's theory. Schoenberg (1980) also represents the effective compliance tensor as

$$\boldsymbol{s}_e^{\mathrm{S}} = \boldsymbol{s}_b + \boldsymbol{s}_f, \tag{17}$$

where $\boldsymbol{s}_f$ is the excess fracture compliance tensor. For a single fracture set with the crack density e_1 and normal to the crack faces pointing in the x_1-direction, $\boldsymbol{s}_f$ has only three nonzero elements, $s_{f,11}$, $s_{f,55}$, and $s_{f,66}$ (we use Voigt notation here). Their expressions are derived in the low crack-density limit by inverting the results of Hudson (1981) for effective stiffnesses (Schoenberg and Douma, 1988):

$$s_{f,11} = \frac{\mathcal{U}_{33}e_1}{\mu_b},\quad s_{f,55} = s_{f,66} = \frac{\mathcal{U}_{11}e_1}{\mu_b}, \tag{18}$$

where

$$\mathcal{U}_{11} = \frac{16}{3(3-2g)(1+\mathcal{M})},\quad \mathcal{U}_{33} = \frac{4}{3(1-g)(1+\mathcal{K})}, \tag{19}$$

$$\mathcal{M} = \frac{4\mu_i}{\pi\theta(3-2g)\mu_b},\quad \mathcal{K} = \frac{\lambda_i+2\mu_i}{\pi\theta(1-g)\mu_b}, \tag{20}$$

$$g = \frac{\mu_b}{\lambda_b+2\mu_b}, \tag{21}$$

and λ_i and μ_i are the Lamé parameters of the infill.

For dry cracks ($\lambda_i = \mu_i = 0$), equations 18 coincide with equations 6, 11, and 12,

$$\boldsymbol{s}_f = \Delta\boldsymbol{s}. \tag{22}$$

Such an equality, however, no longer holds for liquid-filled cracks.

Extension of the above results to L differently oriented fracture sets is accomplished according to the following scheme: the fourth-ranked tensor $\boldsymbol{s}_f$ is replaced with a sum

$$\boldsymbol{s}_f \to \sum_{\ell=1}^{L} \boldsymbol{s}_f^{(\ell)}, \tag{23}$$

where $\boldsymbol{s}_f^{(\ell)}$ are the properly rotated excess-fracture tensors corresponding to the individual fracture sets. Substitution 23 explicitly ignores any influence of details of spatial distribution of fractures on the effective parameters exactly as it should in the noninteraction approximation.

Hudson's theory

In contrast to the formulations of Kachanov and Schoenberg, Hudson (1980) derives the effective stiffness $\boldsymbol{c}_e$ rather than the compliance $\boldsymbol{s}_e$. The stiffness tensor is constructed as a power series with respect to the crack density.

The first-order result of Hudson (1980, 1981) is

$$\boldsymbol{c}_e^{\mathrm{H1}} = \boldsymbol{c}_b + \Delta\boldsymbol{c}, \tag{24}$$

where $\boldsymbol{c}_b = \boldsymbol{s}_b^{-1}$ is the stiffness tensor of the isotropic background rock. The term $\Delta\boldsymbol{c}$ represents the usual noninteraction approximation, that is, the result for compliances which is inverted and linearized with respect to the crack density. For a single set of penny-shaped fractures that has a crack density e_1 and normal $\boldsymbol{n}^{(1)} = [1,0,0]$, $\Delta\boldsymbol{c}$ is given by

$$\Delta \boldsymbol{c} = -\frac{e_1}{\mu_b}\begin{pmatrix} (\lambda_b+2\mu_b)^2\boldsymbol{\mathcal{U}}_{33} & \lambda_b(\lambda_b+2\mu_b)\boldsymbol{\mathcal{U}}_{33} & \lambda_b(\lambda_b+2\mu_b)\boldsymbol{\mathcal{U}}_{33} & 0 & 0 & 0 \\ \lambda_b(\lambda_b+2\mu_b)\boldsymbol{\mathcal{U}}_{33} & \lambda_b^2\boldsymbol{\mathcal{U}}_{33} & \lambda_b^2\boldsymbol{\mathcal{U}}_{33} & 0 & 0 & 0 \\ \lambda_b(\lambda_b+2\mu_b)\boldsymbol{\mathcal{U}}_{33} & \lambda_b^2\boldsymbol{\mathcal{U}}_{33} & \lambda_b^2\boldsymbol{\mathcal{U}}_{33} & 0 & 0 & 0 \\ 0 & 0 & 0 & 0 & 0 & 0 \\ 0 & 0 & 0 & 0 & \mu_b^2\boldsymbol{\mathcal{U}}_{11} & 0 \\ 0 & 0 & 0 & 0 & 0 & \mu_b^2\boldsymbol{\mathcal{U}}_{11} \end{pmatrix}. \tag{25}$$

The quantities $\boldsymbol{\mathcal{U}}_{11}$ and $\boldsymbol{\mathcal{U}}_{33}$ are defined by equations 19 (also Peacock and Hudson, 1990, their equations 2). In the presence of several differently oriented fracture sets, their stiffness contributions $\Delta \boldsymbol{c}^{(\ell)}$ are summed up following recipe 23 (Hudson, 1981).

The second-order theory of Hudson (1980, 1991) extends the linear approximation 24 by adding the quadratic term in the crack density:

$$\boldsymbol{c}_e^{\mathrm{H2}} = \boldsymbol{c}_b + \Delta \boldsymbol{c} + \Delta\Delta \boldsymbol{c}, \tag{26}$$

where

$$\Delta\Delta \boldsymbol{c} = \frac{1}{\mu_b}\Delta \boldsymbol{c} : \boldsymbol{\chi} : \Delta \boldsymbol{c}, \tag{27}$$

$$\chi_{ijkl} = \frac{1}{15}[\delta_{ik}\delta_{jl}(4+g) - (\delta_{il}\delta_{jk} + \delta_{ij}\delta_{kl})(1-g)],$$
$$(i, j, k, l = 1, 2, 3), \tag{28}$$

and g is given by equation 21.

NUMERICAL VERIFICATION OF EFFECTIVE MEDIA THEORIES

The goal of this section is to test the theoretical models discussed above by direct computational studies on a number of arrays of circular cracks. To construct the effective stiffness $\boldsymbol{c}_e^{\mathrm{N}}$, we solve equations of static equilibrium for a microheterogeneous elastic solid with the FEMLAB (Comsol, 2006) finite-element modeling package and follow the methodology described by Grechka (2003, 2005). In addition, we apply both the traction and periodic displacement conditions at outer boundaries of the computational domain. Our typical meshes contain from 100,000 – 500,000 tetrahedron elements. The meshes are generated and adjusted automatically to fit the fracture surfaces and interiors. Normally, about 70% of the finite elements lie inside the cracks and their immediate vicinities, where the stress and strain fields change most rapidly.

For our comparison of theoretical and numeric results to be meaningful, we must maintain randomness of the fracture locations and ensure that the cracks neither overlap nor intersect each other. We meet both of these requirements by inserting the fractures into V randomly in a sequential manner and by accepting each new fracture only after verification that it does not intersect the already existing ones. Still, the crack faces can almost touch each other, and no model volume is excluded artificially.

We compute the effective stiffnesses for a suite of models that contains three vertical fracture sets. The fractures are either dry or filled with water. Parameters of their infills and the background are listed in Table 1. Fracture normals have azimuths $\varphi_1 = 0^\circ$, $\varphi_2 = 20^\circ$, and $\varphi_3 = 60^\circ$ with respect to the coordinate axis x_1. The crack density e_1 of the first set varies from 0 to 0.09, while the densities of other two sets are kept fixed for all models at $e_2 = 0.02$ and $e_3 = 0.03$. This allows us to examine the effective properties as functions of e_1. Once the crack densities of the fracture sets that comprise a given model are specified, we perform 10–15 numeric simulations of effective media by changing the number of cracks and their spatial locations. Our models have from 10–100 individual cracks; their aspect ratios $\theta^{(k)}$ vary randomly in the range $0.05 \le \theta^{(k)} \le 0.15$.

Figure 1 shows a typical field of the stress component $\tau_{11}(\boldsymbol{x})$, where $\boldsymbol{x}_1$ is the direction of uniaxial remote loading. This figure can be regarded as an illustration of strong local disturbances in the field $\tau_{11}(\boldsymbol{x})$ that usually involve several adjacent fractures. Despite that and similar phenomena in two dimensions, which have been known for a long time, Kachanov (1992, 1993) suggests that competing interaction effects of stress shielding (blue) and amplification (yellow and red) largely cancel each other if the centers of cracks are distributed randomly in V. Indeed, Figure 1 demonstrates that the zones of shielding and amplification alternate. The shielding appears to slightly dominate amplification, thus indicating that interactions tend to stiffen the effective medium compared to the predictions given by the noninteraction approximation.

Table 1. Parameters of background and fracture infill. Relationships between the Lamé constants λ and μ, the P- and S-wave velocities V_P and V_S, and the density ρ are given by conventional expressions $\lambda = \rho(V_P^2 - 2V_S^2)$ and $\mu = \rho V_S^2$.

	V_P (m/s)	V_S (m/s)	ρ (kg/m^3)	λ (GPa)	μ (GPa)
Background	2500.0	750.0	2200.0	11.28	1.24
Wet cracks	1500.0	1.0	1000.0	2.25	$1.0 \cdot 10^{-6}$
Dry cracks	330.0	1.0	1.29	1.4×10^{-4}	1.3×10^{-9}

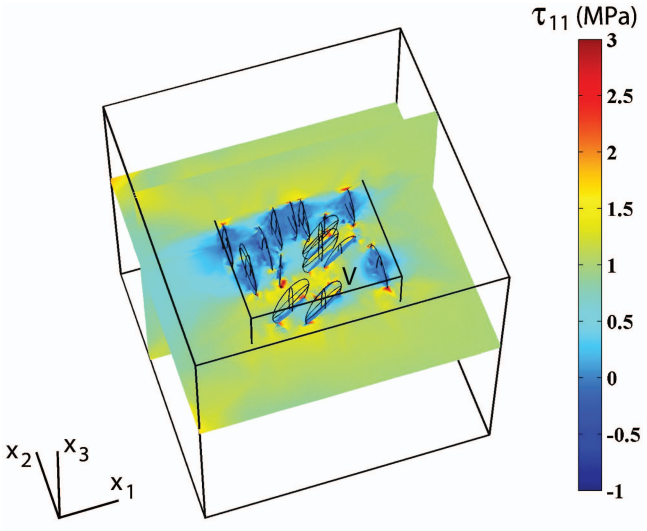

Figure 1. Vertical and horizontal cross sections of stress component $\tau_{11}(\boldsymbol{x})$ through a typical model that contains three dry fracture sets characterized by crack densities $e_1 = 0.09$, $e_2 = 0.02$, and $e_3 = 0.03$ and azimuths $\varphi_1 = 0^\circ$, $\varphi_2 = 20^\circ$, and $\varphi_3 = 60^\circ$. Background and infill parameters are listed in Table 1.

Dry fractures

Let us begin our comparison of effective media theories with models containing vertical dry fractures and then turn our attention to the water-filled fractures. We will not explicitly specify the boundary conditions applied to crack arrays discussed below because the empty volume between the outer model edges and the domain containing the cracks (Figure 1) effectively eliminates the influence of boundary conditions on the results of our computations. The effective media caused by vertical fractures are monoclinic with a horizontal symmetry plane. Their description can be simplified in a specially chosen coordinate frame $\tilde{\boldsymbol{x}}_k$. The $\tilde{\boldsymbol{x}}_1$ and $\tilde{\boldsymbol{x}}_2$ axes of this new frame point along the polarization vectors of two vertically propagating shear waves [this makes the effective stiffness coefficient $c_{e,45}$ vanish, e.g., Grechka et al. (2000)], and the $\tilde{\boldsymbol{x}}_3$-axis is vertical.

Comparison of theoretical predictions

Figure 2 shows predictions of the effective stiffness component $c_{e,11}(e_1)$ made by different theories. Its most notable feature is that all theories except those of Hudson (marked with $\triangleleft$ and $\triangleright$) indicate similar behavior of $c_{e,11}(e_1)$ and closely match the results of finite-element computations ($\times$). Clearly, both first- and second-order Hudson's theories are in significant error. His first-order theory (equations 24 and 25) yields negative $c_{e,11}$ values at $e_1 \gtrsim 0.035$. This feature is also observed for a single fracture set (Appendix A).

The second-order theory of Hudson (equations 26–28, marked with $\triangleright$) results in monotonically growing $c_{e,11}(e_1)$, which implies that adding fractures stiffens rather than softens the rock. This theory leads to another, equally unphysical prediction: $c_{e,11}$ exceeds the corresponding background value $c_{b,11} = \lambda_b + 2\mu_b = 13.75$ GPa (Table 1) at $e_1 \gtrsim 0.03$, thus indicating that a solid containing fractures is stiffer than the uncracked one. The tendency of the second-order Hudson's theory to produce the unreasonably high effective stiffness displayed in Figure 2 has been known for a long time, both for a single fracture set and for randomly oriented cracks (Sayers and Kachanov, 1991; Cheng, 1993). Jakobsen et al. (2003) show that the same tendency holds for an arbitrary distribution of fractures.

Figure 2 illustrates how unfavorably Hudson's predictions compare with those of others. For this reason, we refrain from displaying Hudson's results in Figures 3–5 and 7 for dry cracks; oftentimes, his theory predicts the effective properties that fall out of the scale ranges of our plots. Figure 2 also indicates that theories of Schoenberg ($\star$) and various modifications of Kachanov's theory ($\bigcirc$, $\triangle$, and $\triangledown$) yield very similar values of $c_{e,11}$. To see these differences better and to relate our computations to seismic signatures more directly, hereinafter we present the elastic properties of effective monoclinic media in terms of the vertical velocities and Thomsen-style anisotropic coefficients introduced by Grechka et al. (2000).

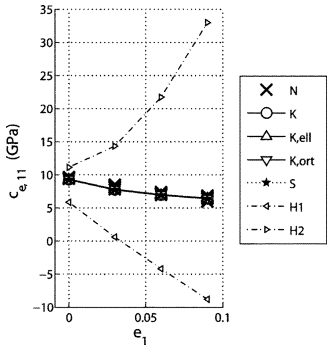

Figure 2. Effective stiffness component $c_{e,11}(e_1)$. The legend indicates the methods applied to compute $c_{e,11}$, listed in Table 2.

Figures 3 and 4 show the effective parameters that fully characterize monoclinic media obtained with different theories. Similarly to Kachanov (1992) and Grechka (2005) we observe that the theories always predict unique effective values for any given crack density e_1, whereas the results of finite-element computations (marked with $\times$) exhibit some scatter. The reason for this scatter lies in the finite number of cracks (from 10 to 100) used in our simulations.

Concerning Figures 3 and 4, let us observe the following:

- While all theories overestimate the shear-wave vertical velocity (Figure 3b), the elliptical approximation of Kachanov ($\triangle$, equation 14) encounters greater errors. Such a result stems from ignoring the nonzero crack aspect ratios by the theories. It can be shown that theories that take finite $\theta^{(k)}$ into account (e.g., Mori and Tanaka, 1973; Kachanov and Sevostianov, 2005) are much more successful in predicting the behavior of $V_{S0}(e_1)$ displayed in Figure 3b.
- As follows from equation 22, we observe no difference between the theory of Kachanov ($\bigcirc$) and the linear slip theory of Schoenberg ($\star$).
- Given typical errors in the interval velocities and anisotropic coefficients estimated from seismic data, theoretical predictions of both Kachanov and Schoenberg are satisfactory.

Elliptical anisotropy and orthotropy

Now we turn our attention to the ellipticity of effective anisotropy established by the simplified theory of Kachanov (equation 14). Figures 3d, 3e, 3g, and 3h reveal that $\boldsymbol{\epsilon}^{(1)} \approx \boldsymbol{\delta}^{(1)}$ and $\boldsymbol{\epsilon}^{(2)} \approx \boldsymbol{\delta}^{(2)}$. To assess the anellipticity of effective anisotropy quantitatively, we examine the coefficients $\eta^{(1)}$, $\eta^{(2)}$, and $\eta^{(3)}$ displayed in Figure 5. The greatest absolute value obtained in finite-element modeling is about 0.02 for $\eta^{(1)}$ (Figure 5a). Such a small anellipticity can easily go unnoticed in seismic data. Therefore, the effective anisotropy is essentially elliptic for seismic applications.

Table 2. Symbols that mark results of effective media theories in Figures 2–6 and 6–12.

Symbol	Theory or its approximation	Equations
$\times$ – N	Numerical (finite element) modeling	
$\bigcirc$ – K	Theory of Kachanov	6, 10
$\triangle$ – K,ell	Theory of Kachanov, $\approx$ elliptical anisotropy	5, 14
$\triangledown$ – K,ort	Theory of Kachanov, $\approx$ orthotropy	15, 16
$\star$ – S	Theory of Schoenberg	17–23
$\triangleleft$ – H1	First-order theory of Hudson	24, 25
$\triangleright$ – H2	Second-order theory of Hudson	25–28

Approximations 14 (△), 15, and 16 (▽) indicate that the symmetry of effective media is orthorhombic. This statement is justified by Figure 4, which shows deviations from orthotropy quantified by the anisotropic coefficients $\zeta^{(1)}$, $\zeta^{(2)}$, and $\zeta^{(3)}$. Clearly, the magnitudes of all $\zeta^{(i)}$ are smaller than those of other anisotropic coefficients. Are they small enough for seismics? This question can be addressed by looking at the NMO ellipses from a horizontal reflector whose misalignments give another measurement of the difference between orthorhombic and monoclinic symmetries (Grechka et al., 2000). Figure 6 displays these ellipses for the largest crack density $e_1 = 0.09$ used in our computations. It indicates that the azimuths of semiaxes of numerically computed NMO ellipses (solid) are close to the polarization directions (0° and 90°) of vertically propagating split shear waves. Therefore, numerically computed effective media are orthorhombic for seismic reflection data. The NMO ellipses for other crack densities (not shown) reinforce this conclusion.

Let us note that orthotropic approximation (marked with ▽ in Figure 6) predicts the numerically computed P-wave NMO ellipses quite well; however, it somewhat overestimates the shear-wave NMO velocities (Figures 6b and 6c). This bias can be tracked back to the correspondingly higher vertical S-wave velocity V_{S0} (Figure 3b).

Perhaps a final judgment about the proximity of theoretically predicted and numerically computed effective media to orthotropy can be made based on magnitudes of the relative ℓ_2 norms:

$$\Delta_e^{\text{orth}} = \frac{||\boldsymbol{c}_e - \boldsymbol{c}_e^{\text{orth}}||}{||\boldsymbol{c}_e||} \times 100\%, \tag{29}$$

where $\|\boldsymbol{c}\| = (\sum_{i,j,k,l=1}^{3} c_{ijkl}^2)^{1/2}$ and tensors $\boldsymbol{c}_e^{\text{orth}}$ are obtained from $\boldsymbol{c}_e$ by letting

$$c_{e,ijkl}^{\text{orth}} = \begin{cases} 0 \text{ when} \\ \delta_{ij}\delta_{kl} + \delta_{ik}\delta_{jl} + \delta_{il}\delta_{kj} = 0 \\ \text{and} \\ c_{e,ijkl} \text{ otherwise} \\ (i, j, k, l = 1, 2, 3). \end{cases} \tag{30}$$

Figure 7 demonstrates that all relative norms Δ_e^{orth} are less than 1.4%. To understand whether these deviations from orthotropy are large enough from a seismic perspective, one must remember that errors in estimating in-situ stiffness components, for instance, from multicomponent, multiazimuth, walkaway vertical seismic profiling (VSP) data are expected to be in the range of 5%–10% for good-quality measurements (e.g., Dewangan and Grechka, 2003). Therefore, the differences between $\boldsymbol{c}_e$ and $\boldsymbol{c}_e^{\text{orth}}$ shown in Figure 7 can be safely ignored, because they are too small to be resolved from seismic data.

To summarize our study of media with multiple sets of vertical dry cracks, we state that their effective anisotropy is ac-

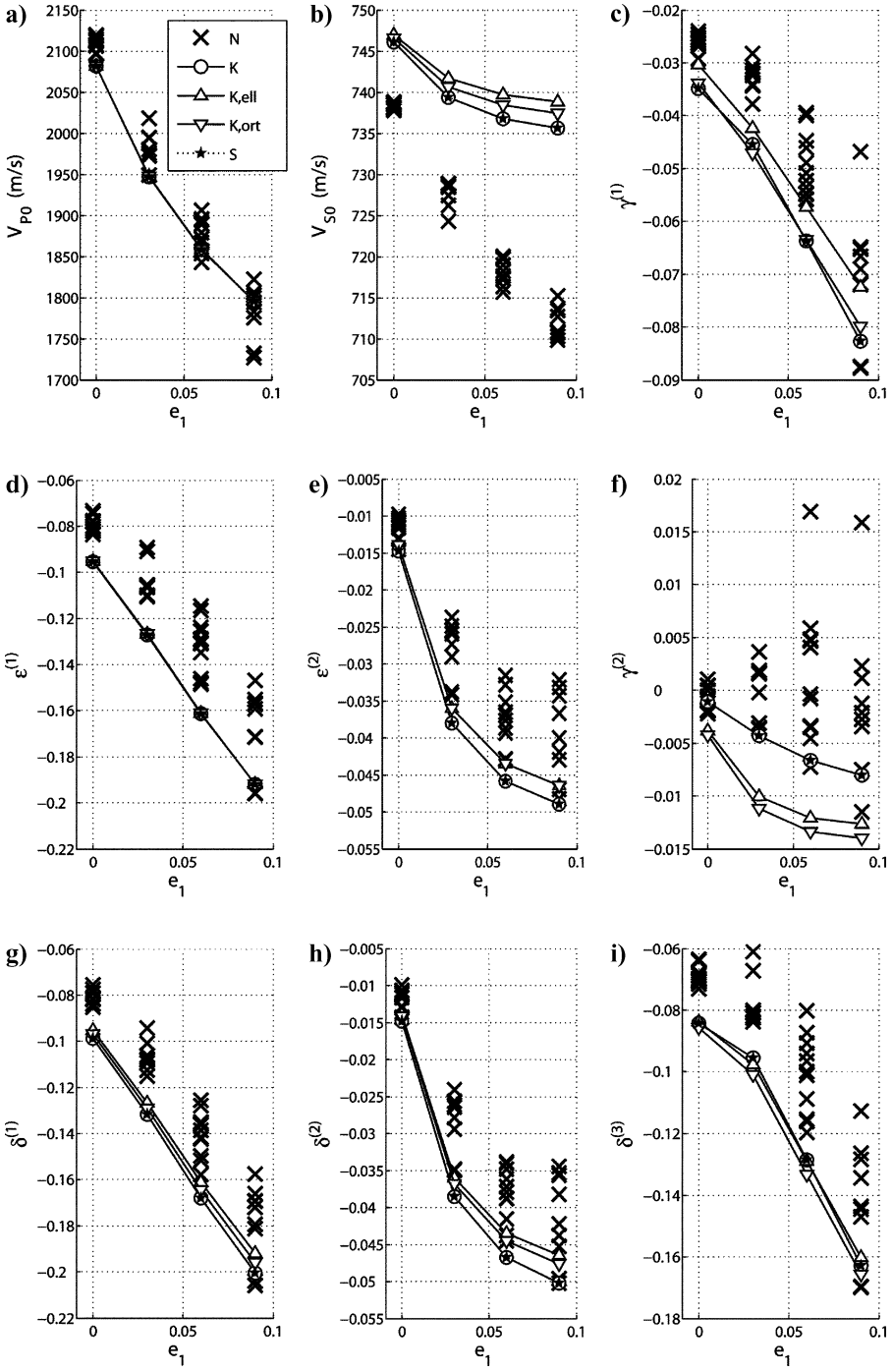

Figure 3. Effective vertical velocities and anisotropic coefficients. Symbols that mark results of various effective media theories are listed in Table 2.

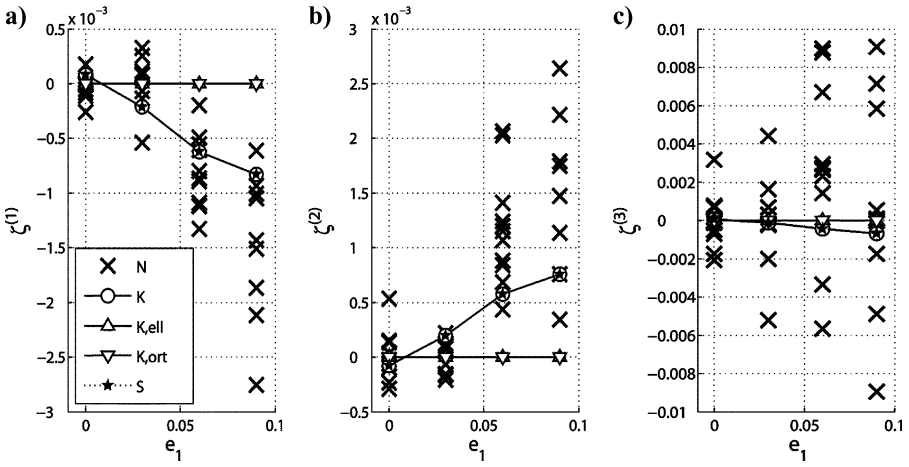

Figure 4. Effective anisotropic coefficients $\zeta^{(1)}$, $\zeta^{(2)}$, and $\zeta^{(3)}$ that express the deviations of monoclinic media from orthotropy.

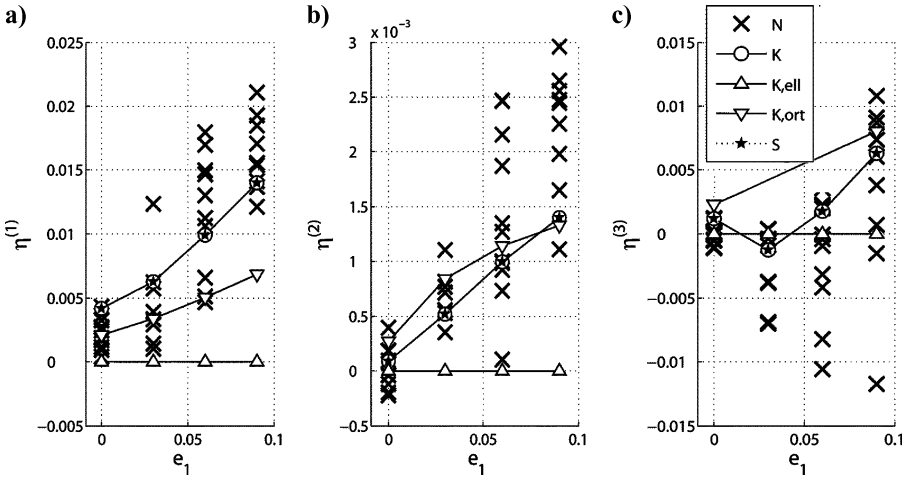

Figure 5. Effective anellipticity coefficients $\eta^{(1)}$, $\eta^{(2)}$, and $\eta^{(3)}$. Methods used to obtain $\eta^{(1,2,3)}$ are marked with symbols given in Table 2.

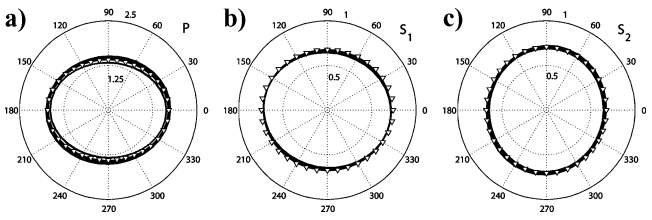

Figure 6. Exact NMO ellipses of (a) P-, (b) S_1-, and (c) S_2-waves computed from $\boldsymbol{c}_e^{\mathrm{N}}$ (solid). Symbols $\triangledown$ denote the same exact NMO ellipses but are obtained using approximations 15 and 16. All computations are done for models that have the crack density e_1 = 0.09. Numbers along vertical radii indicate NMO velocities (in kilometers/second); numbers around outer circles correspond to azimuths (in degrees) from polarization direction of the vertically propagating fast shear wave.

curately approximated by the elliptical orthotropy. The physical reason for it is the closeness of the fracture compliances in the directions normal and tangential to the crack faces. This closeness exhibits itself in the dominance of the second-rank crack-density tensor $\boldsymbol{\alpha}$ over the fourth-rank tensor $\boldsymbol{\beta}$ (equation 1). As a result, deviations from orthotropy can hardly be observed from seismics even when multiazimuth, multicomponent data are available. Similar computations performed for another suite of models that contains four rather than three sets of penny-shaped fractures (not shown here) substantiate our conclusion. We also extended this work to more realistic noncircular and intersecting cracks. Such complicated fracture geometries do not invalidate the effective orthotropy and yield the deviations Δ_e^{orth} that have similar magnitudes to those shown in Figure 7. We will report details of our study in a sequel paper.

Water-filled fractures

Now we compare the effective media theories with finite-element computations for fractures filled with water. The results for vertical velocities and anisotropic coefficients are displayed in Figures 8 and 9. Several observations are in order. First, the magnitude of crack-induced anisotropy is much smaller than that for dry fractures (Figure 3). Second, because of the mild anisotropy discrepancies between different theories become less pronounced. As a consequence, Hudson's

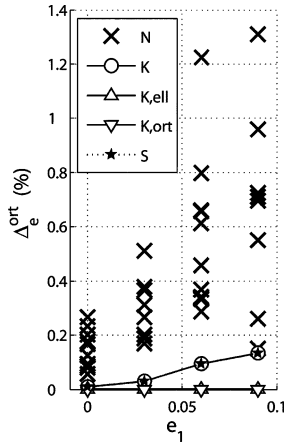

Figure 7. Relative deviations of the effective stiffness tensors from orthotropy.

predictions may be viewed as acceptable, although his first-order results (◁) are still among the worst (Figures 8a, 8d, 8e, 8g, and 8h). Third, predictions of the linear slip theory (⋆) are not as good as they were for dry fractures (compare Figures 3a and 8a, 3d and 8d, 3e and 8e, 3g and 8g, and 3h and 8h). We believe this is because the excess fracture compliances were obtained by Schoenberg and Douma (1988) by inverting Hudson's (1980, 1981) first-order results for the stiffnesses. Finally, it appears that theory of Kachanov (○) fits finite-element computations (×) slightly better than do the other theories. This, however, is not important because errors encountered by all the theories are small by seismic standards.

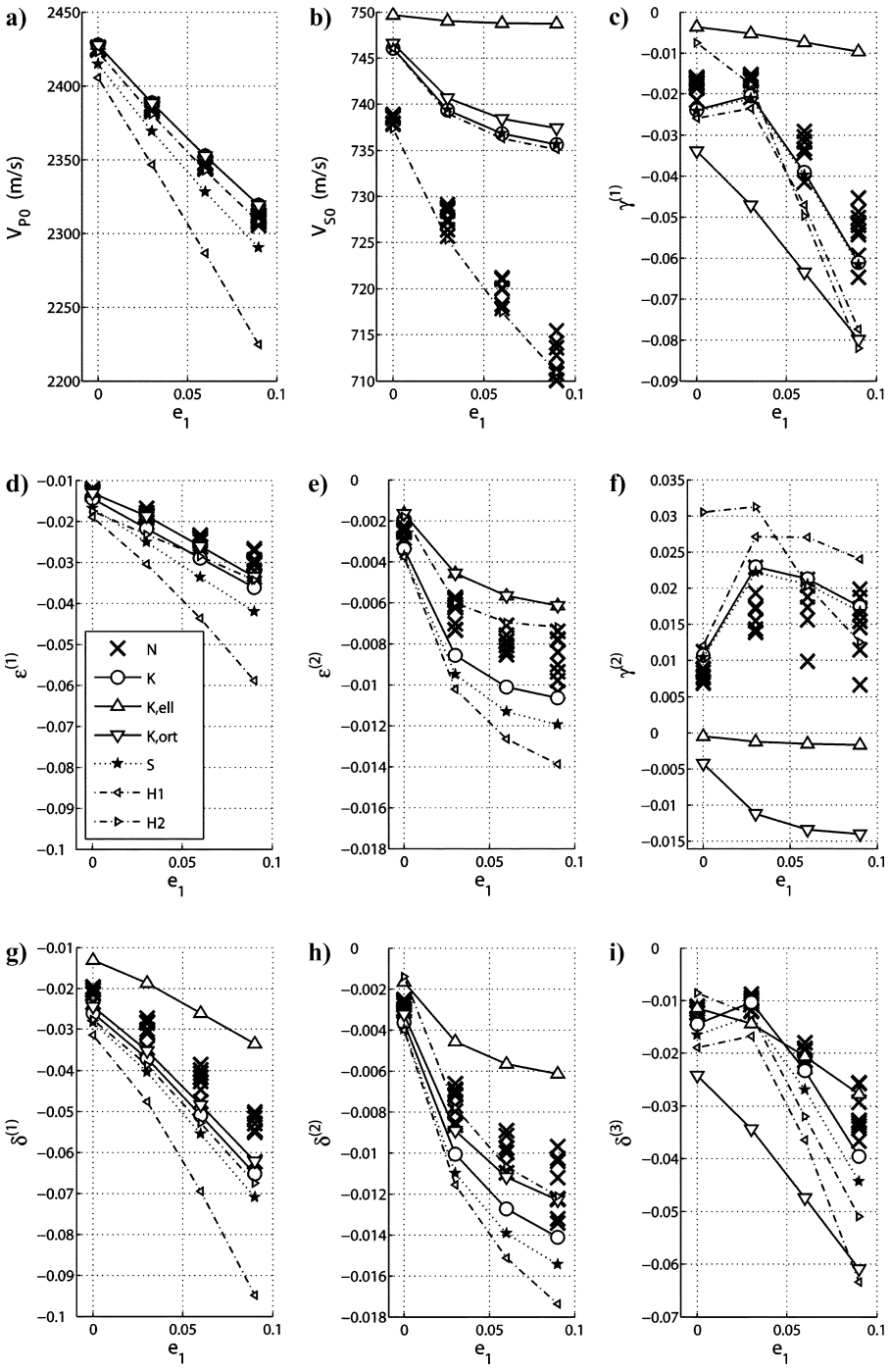

Figure 8. Same as Figure 3 but for water-filled cracks.

Elliptical anisotropy?

While in general we do not expect anisotropy to be elliptical for wet cracks, it is still instructive to check the closeness of numerically generated effective media to elliptically anisotropic ones. Figure 10 displays the theoretical anellipticity coefficients along with their values resulting from our finite-element computations. On the one hand, the absolute maximum of $|\eta^{(1)}| = 0.033$ (Figure 10a) is rather small to be called sizeable for seismics; on the other, it is greater than that observed for dry fractures (Figure 5). Therefore, we suggest that anellipticity of effective anisotropy might be used to discriminate fluid infill of fractures; however, it is not particularly sensitive to its type.

Orthotropy

Although elliptical anisotropy holds only approximately for water-filled fractures, the symmetry of effective media is close to orthorhombic. This statement is supported by the small values of ζ-coefficients (Figure 9) and by comparing the azimuths of semiaxes of pure-mode NMO ellipses from a horizontal reflector (Figure 11) with the polarization directions of vertically propagating shear waves (0° and 90°). The maximum azimuthal misalignment between the ellipse orientations and the shear-wave polarization directions of 12° observed for the S_1-wave in Figure 11b is similar to that we had for dry cracks (9° for S_2-wave in Figure 6c). Comparison of Figures 11b and 11c with Figures 6b and 6c reveals that the accuracy of approximations 15 and 16 degrades when gas filling the fractures is replaced with water. This happens because the approximation ignores a portion of the relatively strong contribution of the fourth-rank tensor $\boldsymbol{\beta}'$ to the effective stiffnesses and the influence of diverse aspect ratios.

Figure 12 gives an answer to the question of closeness of numerically computed effective stiffness tensors to orthotropy. The absolute maximum of their deviations (×) is just 0.3%. Clearly, the orthotropy of effective media is well justified. It is caused, however, by a rela-

tively weak crack-induced anisotropy whose deviations from the isotropic background are small.

FRACTURE CHARACTERIZATION

Comparison of various effective media theories with finite-element modeling done in the previous section led us to an important conclusion: Rocks containing multiple fracture sets are almost orthotropic. Moreover, we noticed that, for dry cracks, effective orthotropy has a greatly simplified type. Instead of nine independent parameters, it is fully characterized by only four: Lamé constants λ_b and μ_b of the isotropic background and two principal crack densities $\widetilde{e}_1$ and $\widetilde{e}_2$. (This means, in particular, that the effective shear stiffnesses $c_{e,44}$, $c_{e,55}$, and $c_{e,66}$ are not independent; they can be expressed in terms of the other effective stiffness coefficients.) We also speculated that the average fluid factor ς might be used to indicate the presence of fluids, thus bringing the total number of governing parameters to five. Since our fracture sets are vertical, one of the symmetry planes of effective orthorhombic media is always horizontal. Azimuths of the two vertical planes are given by the eigenvectors of tensor $\boldsymbol{\alpha}$; they coincide with polarization directions of two vertically propagating split shear waves.

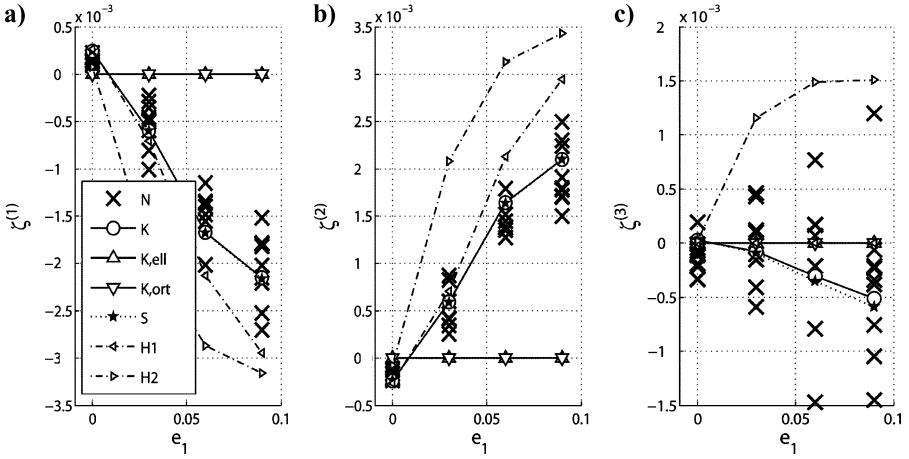

Figure 9. Same as Figure 4 but for water-filled cracks.

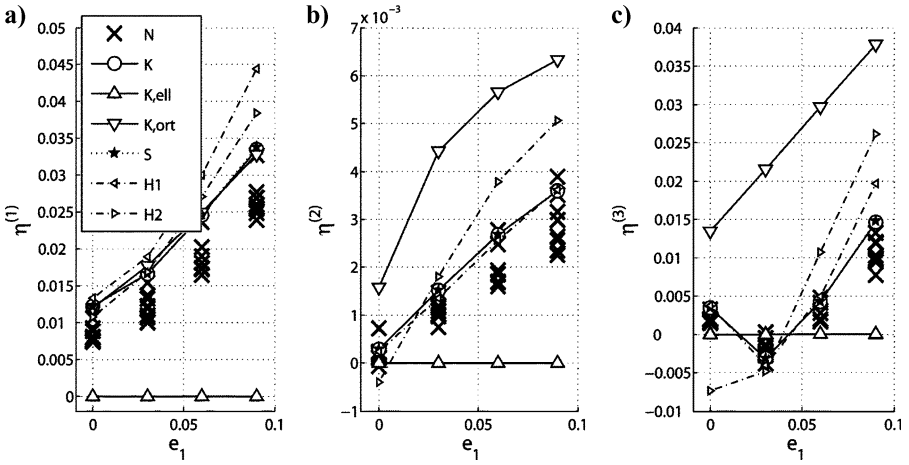

Figure 10. Effective anellipticity coefficients $\eta^{(1)}$, $\eta^{(2)}$, and $\eta^{(3)}$ for water-filled fractures.

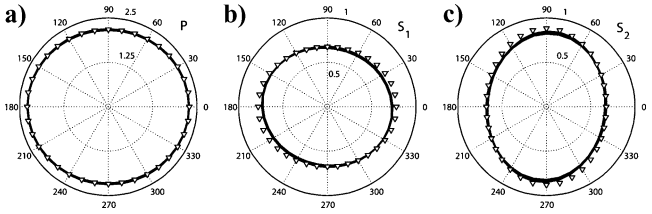

Figure 11. Same as Figure 6 but for wet fractures: (a) P-, (b) S_1-, and (c) S_2-waves.

Here we use the numerically computed effective stiffness tensors $\boldsymbol{c}_e^{\mathrm{N}}$ to generate seismic signatures. This is done under conventional assumption that seismic wavelengths are much greater than the fracture sizes and, therefore, the static effective media theories are applicable. We would like to estimate the parameter vector

$$\boldsymbol{M} = \{\lambda_b, \mu_b, \widetilde{e}_1, \widetilde{e}_2, \varsigma\} \qquad (31)$$

from seismic data. While a variety of seismic signatures can be used for such an inversion, here we choose those that are measurable from reflection data and therefore make it possible to map the fracture attributes 31 remotely. Thus, our data vector is

$$\boldsymbol{D} = \left\{ \frac{V_{S1}}{V_{P0}},\ \frac{V_{S2}}{V_{P0}},\ \boldsymbol{W}^{Q} \right\},$$
$$(Q = P, S_1, S_2), \qquad (32)$$

where $\boldsymbol{W}^{Q}$ are the NMO ellipses of P-, S_1-, and S_2-waves recorded from a horizontal reflector; V_{S1} and V_{S2} are the vertical velocities of fast and slow shear waves; and the ratios V_{S1}/V_{P0} and V_{S2}/V_{P0} are obtained from the ratios of the corresponding zero-offset times after establishing the P- and shear-wave event correspondence.

We calculate the data vector $\boldsymbol{D}(\boldsymbol{c}_e^{\mathrm{N}})$ exactly and then use approximations 15 and 16 to compute $\boldsymbol{D}(\boldsymbol{M})$ for a trial vector $\boldsymbol{M}$ (equation 31). The unknown components of $\boldsymbol{M}$ are found by minimizing the nonlinear objective function

$$\mathcal{F} = \min_{(\boldsymbol{M})} \left\| \boldsymbol{D}(\boldsymbol{c}_e^{\mathrm{N}}) - \boldsymbol{D}(\boldsymbol{M}) \right\|. \qquad (33)$$

Figures 13–15 show the output of our inversion for all numerically computed $\boldsymbol{c}_e^{\mathrm{N}}$. We discuss these results next.

Figure 13 displays the inverted background constants λ_b and μ_b ($\times$) and compares them with the corresponding model values

(solid lines). The coefficient μ_b is estimated more accurately than λ_b. Perhaps this is because two shear waves (fast and slow) and only one P-wave are used in the inversion, so the shear modulus gets constrained more tightly. We also observe that λ_b is estimated better when cracks are dry (Figure 13a) then when they are filled with water (Figure 13b). This has to do with a higher accuracy of approximations 15 and 16 for the former.

Estimates of the average fluid factor ς are presented in Figure 14. While scatter of the inverted ς values ($\times$) is noticeable, the message communicated by Figure 14 is certainly optimistic. Indeed, the cloud of estimated ς in Figure 14a is well separated from that in Figures 14b. Thus, Figure 14 demonstrates that seismic signatures 32 are capable of distinguishing the type of fluid infill.

Finally, Figure 15 compares theoretical and inverted values of the principal crack densities $\widetilde{e}_1$ and $\widetilde{e}_2$. The main conclusion that follows from Figure 15a is clear: The pure-mode NMO ellipses and ratios of the vertical velocities of P- and shear waves allow us to recognize the presence of more than one dry fracture set. As expected, the accuracy of inverted crack densities in Figure 15a is good. Some of their bias toward smaller $\widetilde{e}_1$ and $\widetilde{e}_2$ values is because

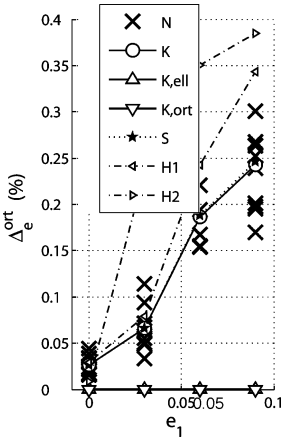

Figure 12. Relative deviations of effective stiffness tensors from orthotropy (equations 29 and 30) for fractures filled with water.

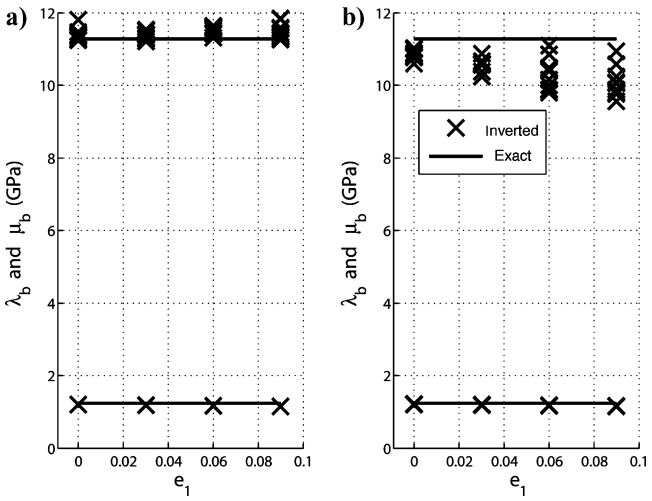

Figure 13. Background Lamé constants λ_b and μ_b for (a) dry and (b) water-filled cracks. Solid lines indicate the exact values of λ_b and μ_b (Table 1), $\times$ indicates the inverted ones.

of finite crack aspect ratios, which are ignored by the applied approximations 15 and 16.

The bias of estimates $\widetilde{e}_1$ and $\widetilde{e}_2$ grows when fractures are filled with water (Figure 15b) because of the inherent ambiguity of the inversion. As we mentioned earlier, proper fracture characterization would require obtaining the aspect ratios of each individual crack — something that cannot be done in a unique fashion. We attempt to overcome this nonuniqueness by relying on equations 15 and 16, which can be viewed as a dry-crack approximation of stiffer liquid-filled fractures. However, the contribution of fractures to effective properties is dominated by the cracks with larger aspect ratios that constitute only a portion of the crack population. This obviously results in smaller crack densities that fit the effective stiffnesses (Figure 15b).

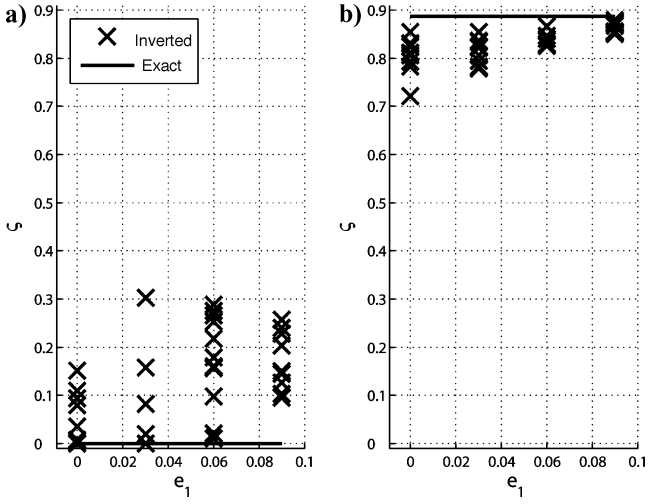

Figure 14. Fluid factors ς for (a) dry and (b) water-filled cracks. Solid lines and $\times$ indicate the model and inverted values of ς, respectively.

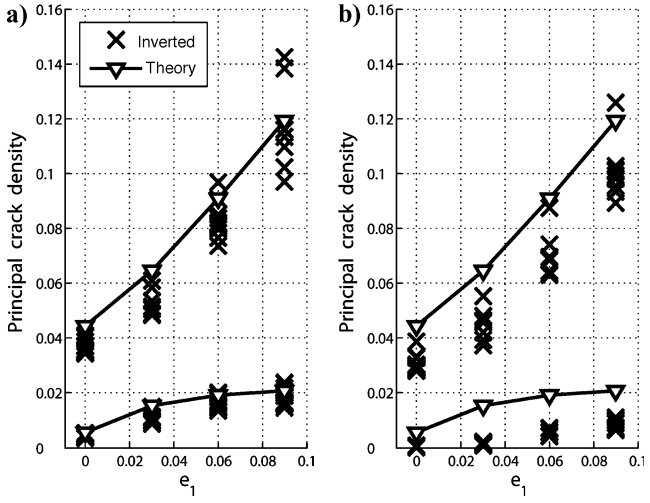

Figure 15. Principal crack densities $\widetilde{e}_1$ and $\widetilde{e}_2$ for (a) dry and (b) water-filled cracks. Symbols $\times$ and $\triangledown$ indicate the inverted and theoretical values of $\widetilde{e}_k$, respectively. The latter are computed as nonzero eigenvalues of tensor $\boldsymbol{\alpha}$ (equation 2).

DISCUSSION

Different effective-media theories for fractured solids proposed both in geophysics and solid mechanics predict significantly different overall elastic properties. We feel that about the only way to judge their quality is to check their results against independent numeric simulations of cracked media. Following this philosophy, we consistently compared theories of Hudson, Schoenberg, and Kachanov with finite-element computations for models containing several sets of vertical, nonintersecting fractures. To facilitate comparison of numeric and theoretical results, we deliberately chose cracks that had shapes of circular, thin, oblate ellipsoids. Our main finding was that predictions of both the first- and second-order Hudson's theories are, on average, less accurate than those of Schoenberg and Kachanov. Having established that, we gave our preference to Kachanov's theory because it yielded especially simple description of effective media. It explicitly indicated that effective anisotropy was almost orthorhombic (orthotropic) for all examined models.

An additional and perhaps more important reason for selecting Kachanov's theory for fracture characterization was that it allowed us to identify the proper governing parameters of effective media. As follows from this theory, the number of those parameters is only four for dry cracks. Two of them are the elastic constants of the isotropic host rock. The influence of fractures is captured by the two remaining parameters — the principal components of the crack-density tensor. They reflect, in an integral way, all information about crack orientations and density relevant for low-frequency seismic waves. Importantly, the aspect ratios do not matter for dry fractures as long as the former remain small (below about 0.10–0.15). For fluid-filled cracks, the aspect ratios are important; the overall elastic properties depend on the fracture infill via a dimensionless parameter that incorporates both aspect ratios and fluid compressibility. It should be added to the list of governing parameters.

CONCLUSIONS

To summarize, we have shown that regardless of the number of fracture sets embedded in otherwise isotropic host rock as well as their orientations and types of fluid infill, the symmetry of effective media is approximately orthorhombic. This approximation is expected to be satisfactory for seismic needs because the deviations from orthotropy are smaller than uncertainties (typically exceeding 0.05) in the interval Thomsen-type anisotropic coefficients estimated from seismic data. As predicted by the noninteraction approximation, the effective orthotropy induced by dry vertical fractures is governed by four quantities even when interaction in the stress fields of adjacent cracks is strong. These four quantities are two Lamé constants of the isotropic background and two principal crack densities. If the influence of fluids is described by a single additional quantity, the average fluid factor, the details of microstructure cannot be inferred from effective elastic parameters but the type of fluid infill can. Finally, nonlinear inversion of the P- and S-wave NMO ellipses for fracture parameters demonstrates that characterization of multiple sets of vertical dry fractures is feasible and unique. Such an inversion requires acquiring 3D, multiazimuth, multicomponent seismic data.

ACKNOWLEDGMENTS

The authors thank Shell International E & P, Inc. for permission to publish this paper. We also appreciate useful suggestions made by GEOPHYSICS associate editor Martin Landrø, Colin Sayers, and two anonymous reviewers.

APPENDIX A

ELASTIC STABILITY CONDITIONS AND THE FIRST-ORDER HUDSON'S THEORY

In this appendix, we show how easily predictions of the first-order Hudson's theory (Hudson, 1980; 1981; Peacock and Hudson, 1990) can go wrong and yield a negative-effect stiffness for media containing dry cracks. For simplicity, we limit our discussion here to a single set of vertical, penny-shaped fractures.

We choose coordinate axis x_1 to be normal to the fracture faces, $\boldsymbol{n} = [1,0,0]$, and examine the quantity

$$c_{e,11} = c_{b,11} + c_{11}^{\Delta}, \tag{A-1}$$

where $c_{b,11} = \lambda_b + 2\mu_b$ and c_{11}^{Δ} is given by the element $[1,1]$ of matrix 25 and by the second equation 19 with $\boldsymbol{\mathcal{K}} = 0$ because the fractures are dry. Taking these equations into account, we rewrite equation A-1 as

$$c_{e,11} = (\lambda_b + 2\mu_b)\left[1 - \frac{4e_1}{3g(1-g)}\right]. \tag{A-2}$$

The second term in the brackets of equation A-2 exactly coincides with the third equation 21 of Hudson (1981) or with equations 20a and 24b of Liu et al. (2000).

Next, we find such a crack density e_1 that yields

$$c_{e,11} < 0. \tag{A-3}$$

Combining equation A-2 with inequality A-3 and noting that $\lambda_b + 2\mu_b > 0$ and $g = V_{S,b}^2/V_{P,b}^2 < 3/4$, we obtain

$$e_1 > \frac{3}{4}g(1-g). \tag{A-4}$$

Thus, for a velocity ratio $V_{S,b}/V_{P,b} = 0.3$ typically observed in sedimentary rocks (e.g., Grechka et al., 2002; Grechka and Dewangan, 2003), the first-order Hudson's theory yields negative $c_{e,11}$ when the density of dry fractures exceeds $e_1 \approx 0.06$.

REFERENCES

Bakulin, A., V. Grechka, and I. Tsvankin, 2000, Estimation of fracture parameters from reflection seismic data, parts I–III: Geophysics, **65**, 1788–1830.

Benveniste, Y., 1986, On the Mori-Tanaka method in cracked solids: Mechanics Research Communications, **13**, 193–201.

Bristow, J. R., 1960, Microcracks and the static and dynamic elastic constants of annealed and heavily cold-worked metals: British Journal of Applied Physics, **11**, 81–85.

Cheng, C. H., 1993, Crack models for a transversely isotropic medium: Journal of Geophysical Research, **98**, 675–684.

Comsol, 2006, Femlab reference materials, accessed March 2006. www.comsol.com.
Dewangan, P. and V. Grechka, 2003, Inversion of multicomponent, multiazimuth, walkaway VSP data for the stiffness tensor: Geophysics, **68**, 1022–1031.
Grechka, V., 2003, Effective media: A forward modeling view: Geophysics, **68**, 2055–2062.
———, 2005, Penny-shaped fractures revisited: Studia Geophysica et Geodaetica, **49**, 367–383.
Grechka, V., P. Contreras, and I. Tsvankin, 2000, Inversion of normal moveout for monoclinic media: Geophysical Prospecting, **48**, 577–602.
Grechka, V., and P. Dewangan, 2003, Generation and processing of pseudoshear-wave data: Theory and case study: Geophysics, **68**, 1807–1816.
Grechka, V., and I. Tsvankin, 2003, Feasibility of seismic characterization of multiple fracture sets: Geophysics, **68**, 1399–1407.
Grechka, V., I. Tsvankin, A. Bakulin, J. O. Hansen, and C. Signer, 2002, Joint inversion of PP and PS reflection data for VTI media: A North Sea case study: Geophysics, **67**, 1382–1395.
Hudson, J. A., 1980, Overall properties of a cracked solid: Mathematical Proceedings of the Cambridge Philosophical Society, **88**, 371–384.
———,1981, Wave speeds and attenuation of elastic waves in material containing cracks: Geophyiscal Journal of the Royal Astronomical Society, **64**, 133–150.
———, 1991, Overall properties of heterogeneous material: Geophysical Journal International, **107**, 505–511.
———, 1994, Overall properties of a material with inclusions or cavities: Geophysical Journal International, **117**, 555–561.
Jakobsen, M., J. A. Hudson, and T. A. Johansen, 2003, *T*-matrix approach to shale acoustics: Geophysical Journal International, **154**, 533–558.
Kachanov, M., 1980, Continuum model of medium with cracks: Journal of the Engineering Mechanics Division, ASCE, **106**, 1039–1051.
———, 1992, Effective elastic properties of cracked solids: Critical review of some basic concepts: Applied Mechanics Review, **45**, 304–335.
———, 1993, Elastic solids with many cracks and related problems, in J. W. Hutchinson and T. Wu eds., Advances in applied mechanics, **30**, 259–445.
Kachanov, M., and I. Sevostianov, 2005, On quantitative characterization of microstructures and effective properties: International Journal of Solids and Structures, **42**, 309–336.
Liu, E., J. A. Hudson, and T. Pointer, 2000, Equivalent medium representation of fractured rock: Journal of geophysical Research, **105**, 2981–3000.
Mori, T., and K. Tanaka, 1973, Average stress in matrix and average energy of materials with misfitting inclusions: Acta Metallurgica, **21**, 571–574.
Nichols, D., F. Muir, and M. Schoenberg, 1989, Elastic properties of rocks with multiple sets of fractures: 59th Annual International Meeting, SEG, Expanded Abstracts, 471–474.
O'Connell, R. J., and B. Budiansky, 1974, Seismic velocities in dry and saturated cracked solids: Journal of Geophysical Research, **79**, 5412–5426.
Peacock, S., and J. A. Hudson, 1990, Seismic properties of rocks with distributions of small cracks: Geophysical Journal International, **102**, 471–484.
Saenger, E. H., O. S. Krüger, and S. A. Shapiro, 2004, Effective elastic properties of randomly fractured soils: 3D numerical experiments: Geophysical Prospecting, **52**, 183–195.
Sayers, C. M., and M. Kachanov, 1991, A simple technique for finding effective elastic constants of cracked solids for arbitrary crack orientation statistics: International Journal of Solids and Structures, **27**, 671–680.
———, 1995, Microcrack-induced elastic wave anisotropy of brittle rocks: Journal of Geophysical Research, **100**, 4149–4156.
Schoenberg, M., 1980, Elastic wave behavior across linear slip interfaces: Journal of the Acoustical Society of America, **68**, 1516–1521.
Schoenberg, M., and J. Douma, 1988, Elastic wave propagation in media with parallel fractures and aligned cracks: Geophysical Prospecting, **36**, 571–590.
Schoenberg, M., and K. Helbig, 1997, Orthorhombic media: Modeling elastic wave behavior in a vertically fractured earth: Geophysics, **62**, 1954–1974.
Schoenberg, M., and F. Muir, 1989, A calculus for finely layered anisotropic media: Geophysics, **54**, 581–589.
Schoenberg, M., and C. M. Sayers, 1995, Seismic anisotropy of fractured rock: Geophysics, **60**, 204–211.
Shafiro, B., and M. Kachanov, 1997, Materials with fluid-filled pores of various shapes: Effective moduli and fluid pressure polarization: International Journal of Solids and Structures, **34**, 3517–3540.
Walsh, J. B., 1965a, The effect of cracks on the compressibility of rocks: Journal of Geophysical Research, **70**, 381–389.
———, 1965b, The effect of cracks on uniaxial compression of rocks: Journal of Geophysical Research, **70**, 399–411.